Dalton Transactions

ROYAL SOCIETY OF CHEMISTRY

PAPER

View Article Online
View Journal | View Issue



Cite this: *Dalton Trans.*, 2026, **55**, 2681

# Covalent triazine framework@silica core–shell spheres decorated with ultrafine platinum nanoparticles: a robust catalyst for selective aqueous phase hydrogenation of butane-2,3-dione and pyruvic acid

Claudio Evangelisti, *[a] Werner Oberhauser,*[b] Francesco Poggialini,[a] Emanuela Pitzalis,[a] Xuan Trung Nguyen,[a] Esther Punzi,[a] Serena Coiai, [a] Nicola Scotti, [c] Lorenzo Poggini[b,d] and Alessandro Mandoli [e]

Received 29th October 2025,
Accepted 5th January 2026

DOI: 10.1039/d5dt02604k

rsc.li/dalton

Sub-nanometric Pt nanoparticles, generated by the metal vapor synthesis technique, were supported on covalent triazine framework@silica (CTF@$SiO_2$) core–shell hybrid microspheres obtained through polycondensation reactions at the $SiO_2$ surface. The latter catalyst and a reference system (*i.e.* Pt nanoparticles deposited on bare $SiO_2$ microspheres) were screened under identical experimental conditions for the hydrogenation of butane-2,3-dione and pyruvic acid in water, yielding butane-2,3-diol and lactic acid with high selectivity. A combination of catalytic recycling experiments was conducted with both catalysts, along with transmission electron microscopy and X-ray diffraction analyses performed on both the as-synthesized and recovered catalysts, which confirmed the remarkable role of the CTF shell layer in the stabilization of ultrafine Pt NPs against their aggregation under catalysis as well as in enhancing their catalytic activity.



## 1. Introduction

Since their first report in 2005, covalent organic frameworks (COFs) have received increasing interest in catalysis.[1,2] The ordered structure and the light-element composition of COF-based materials lead to a high specific surface area and adjustable pore sizes. Moreover, their customizable structure allows for the incorporation of various functional groups, making them promising materials for different catalytic applications such as photocatalysis, electrocatalysis, energy storage, and fine chemical production.[1,3,4] Among COFs, covalent triazine frameworks (CTFs) stand out due to their unique porous structure, which is attributed to the 1,3,5-triazine units with π-conjugation properties that enhance their thermal and chemical stability.[5–7] Their high nitrogen content, high surface area, and high porosity make them versatile hosts for catalytically active metal species, ranging from single metal atoms to nanoparticles (NPs).[8,9] In fact, the porosity of the polymeric support layer, along with the favourable electron donor properties of the support, is a prerequisite for high catalytic activity in metal-based heterogeneous catalysis.[10–12] Recently, both noble and non-noble metal NPs like Pd, Pt and Ni[13–15] have been successfully immobilized on CTFs, exhibiting elevated dispersion even at high metal loadings and improved catalytic efficiency and recyclability/durability for selective hydrogenation reactions compared to conventional supports (*e.g.* carbon).

Although different synthesis approaches for CTFs have been developed,[16] the large-scale production of these materials still remains a challenge.[17]

Hybrid particles with a silica core and a CTF porous shell combine the advantages of the shell material and the mechanical stability of silica, significantly reducing the required amount of CTF material. As a consequence, the synthesis of the catalytic support can be easily scaled up. In this work, we present a facile approach to fabricate morphology-controllable CTF shells through polycondensation reactions using $SiO_2$ core spheres as a hard template. Sub-nanometer Pt NPs were

[a]*Institute of Chemistry of OrganoMetallic Compounds, ICCOM-CNR, Via G. Moruzzi 1, 56124 Pisa, Italy. E-mail: claudio.evangelisti@cnnr.it*
[b]*Institute of Chemistry of OrganoMetallic Compounds, ICCOM-CNR, Via Madonna del Piano 10, 50019 Sesto Fiorentino, FI, Italy. E-mail: werner.oberhauser@cnr.it*
[c]*Institute of Science and Chemical Technologies "Giulio Natta", SCITEC-CNR, Via C. Golgi 19, 20133 Milano, Italy*
[d]*Department of Chemistry "U. Schiff" – DICUS – and INSTM Research Unit, University of Florence, Via della Lastruccia 3-13, 50019 Sesto Fiorentino, FI, Italy*
[e]*Department of Chemistry and Industrial Chemistry, University of Pisa, Via G. Moruzzi 13, 56124 Pisa, Italy*

generated by metal vapour synthesis (MVS),[18,19] which allows the synthesis of size-tailored metal NPs regardless of the nature of the support. The CTF@$SiO_2$ system was selected as a carrier for the ultrafine Pt NPs to obtain the Pt/CTF@$SiO_2$ composite (**1**). Pure silica spheres were also used to obtain the Pt/$SiO_2$ system (**2**) as a reference catalytic material. Both heterogeneous catalysts were thoroughly characterized by microscopic, spectroscopic, diffraction and thermogravimetric techniques and then used to promote the hydrogenation of butane-2,3-dione (**2,3-BDO**) and pyruvic acid (**PyA**) in water. The chemoselective conversion of both substrates into butane-2,3-diol and lactic acid, respectively, which are recognized as bio-based platform molecules,[20,21] is challenging, since both substrates undergo undesired side reactions due to their reactivity (*i.e.* dimerization of **2,3-BDO** due to the keto–enol tautomerization[22] and decarboxylation of **PyA**[23]). Hence, the development of an efficient and recyclable hydrogenation catalyst, which operates efficiently at relatively low reaction temperature, thereby preventing high temperature-induced side reactions, would be highly desirable. To this aim, we propose a heterogeneous nitrogen-atom stabilizing support material that efficiently stabilizes Pt NPs, in which Pt–N interfacial interactions promote heterolytic hydrogen splitting, making it ideal for the hydrogenation of polar functional groups.[24,25]

## 2. Experimental

### 2.1 Materials

Mesitylene (98%, Merck®) was distilled over metallic Na and then stored under a dry argon atmosphere. The following reagents were purchased from Merck® and used as received without any further purification: ethanol (purity 99.0%), ammonia solution (25–28%), tetraethoxysilane (TEOS, purity 98.0%), (3-aminopropyl)triethoxysilane (APTES, purity 99.0%), dimethyl sulfoxide (purity 99.7%), terephthalaldehyde (TPA, purity 99.0%), cesium carbonate (purity 99.0%), tetrahydrofuran (THF, purity 99.9% inhibitor free), *n*-pentane (purity 99.0%), **2,3-BDO** and **PyA** were purchased from Aldrich and used as received. Water used for catalytic reactions was bidistilled prior to use.

### 2.2 Synthesis

**Synthesis of $SiO_2$ spheres.** Deionized water (40 mL) and ethanol (240 mL) were mixed at 32 °C for 30 min and then ammonia solution (6.8 mL) was slowly added to this mixture. Afterwards, TEOS (24 mL) was quickly added to the solution and the reaction continued for 5 h, affording monodisperse $SiO_2$ nanospheres, which were washed several times with ethanol, centrifuged and then vacuum dried for 24 h.

**Synthesis of CTF@$SiO_2$.** The covalent triazine framework grafted on silica nanospheres (CTF@$SiO_2$) was synthesized following a previously reported procedure.[26] $SiO_2$ nanospheres (5.0 g) were dispersed in ethanol (900 mL) by sonication. Then, APTES (1.5 mL) and ethanol (100 mL) were mixed and then slowly added to the silica ethanol suspension under vigorous stirring at 32 °C. The reaction continued for 12 h yielding amino group-functionalized silica ($NH_2$–$SiO_2$), which was washed with water and ethanol by centrifugation and redispersion, and dried under vacuum for 24 h. Then, $NH_2$–$SiO_2$ (625 mg) was suspended in DMSO (50 mL) and ultrasonically dispersed at ambient temperature until a uniform suspension was obtained. Afterwards, terephthalaldehyde (TPA, 8.0 mg) was added to the above suspension, which was stirred at 60 °C for 12 h, followed by the addition of 1,4-terephthalamidine dihydrochloride (52.9 mg), synthesized according to ref. 27 (see SI section 1.1 for details), and cesium carbonate (120 mg) at 60 °C. The reaction continued for 12 h at this temperature, before being raised to 80 °C and maintained for an additional 12 h. Then, terephthalaldehyde (25.5 mg), 1,4-terephthalamidine dihydrochloride (171.1 mg) and cesium carbonate (240 mg) were added to the above reaction system and reacted at 100 °C for 24 h. The temperature was then maintained at 120 °C for an additional 24 h. The solid (CTF@$SiO_2$) was washed with $H_2O$ and centrifuged. The obtained solid was then transferred back to the flask, stirred in THF for 2 h, centrifuged, washed again with THF and then dried under vacuum for 1 day (final mass 781 mg).

**Synthesis of Pt NPs.** The synthesis of sub-nanometric Pt NPs was carried out following the metal vapor synthesis (MVS) method.[18] Briefly, Pt vapor generated at $10^{-5}$ mbar by resistive heating was condensed with mesitylene vapor (100 mL) onto the cold walls of a glass reactor maintained at −196 °C (liquid nitrogen) for 1 h. The reactor chamber was then heated to the melting point of the solid matrix (*ca.* −40 °C) and the resulting mesitylene-stabilized Pt metal atoms (95.0 mL, 0.80 mg $mL^{-1}$ Pt, measured by ICP-OES) were kept under an argon atmosphere in a Schlenk tube at −80 °C.

**Synthesis of Pt/CTF@$SiO_2$ (1).** A Pt/mes solution (20 mL) was added to CTF@$SiO_2$ (800 mg) dispersed in mesitylene (10.0 mL) under stirring for 12 h. Afterwards, the solvent was removed and the obtained solid (Pt/CFT@$SiO_2$) was washed with *n*-pentane (3 × 20 mL) and dried under reduced pressure to give **1** (810 mg) as a yellow-brown powder. The Pt loading determined by ICP-OES (2.0%) indicated a nearly quantitative deposition of the metal on the support.

**Synthesis of Pt/$SiO_2$ (2).** The synthesis of **2** was carried out by applying the same synthesis method and using $SiO_2$ spheres (reported in section 2.2) instead of CTF@$SiO_2$, as the support. A quantitative deposition of Pt clusters onto the support was obtained leading to a final Pt loading of 2.0 wt%, as proved by ICP-OES analysis conducted on **2**.

### 2.3 Characterization

Inductively coupled plasma–optical emission spectroscopy (ICP-OES) analyses were carried out with an ICP-optical emission dual view PerkinElmer OPTIMA 8000 apparatus. The Pt/mes solution (0.5 mL) (MVS) was heated over a heating plate in a porcelain crucible to remove the solvent, and the solid residue was digested in aqua regia (2.0 mL) for 6 h. The latter solution was then diluted with ultrapure water (PureLab Pro, 18.2 MΩ cm). For the determination of the catalysts' metal

 

loading, the catalyst (10 mg) was treated with aqua regia (4 mL) and refluxed for 6 h. The suspension was then diluted with ultrapure water and centrifuged to remove the silica residue. Quantification of Pt was obtained by means of a calibration curve obtained with suitably diluted Pt stock solutions. The limit of detection (L.O.D.) calculated for platinum was 2 ppb. In all cases, the results of MVS solution and catalyst loading were highly consistent.

Fourier transform infrared (FT-IR) spectra were recorded in ATR mode on sample powder using a Frontiers FTIR spectrometer (PerkinElmer, Milan, Italy), equipped with a diamond-attenuated total reflectance (ATR) sampling accessory. For each sample, three spectra were recorded in the 4000–600 $cm^{-1}$ spectral range with a 4 $cm^{-1}$ resolution, with 32 scans for the background and the sample.

Nitrogen physisorption isotherms were collected with a Micromeritics ASAP2020 instrument. Prior to the analysis carried out at 77 K, the sample was treated under high vacuum at 200 °C for 2 h.

Powder X-ray diffraction (PXRD) was carried out with a PANalytical powder diffractometer equipped with a copper anode (CuKα-radiation, $\lambda$ = 1.541874 Å) and a PIXcel detector. Samples were prepared on a Si wafer (zero background) and spectra were acquired at $2\Theta$ intervals from 10.0 to 80.0°, with a step size of 0.0263° and a counting time of 167.8 s.

Transmission Electron Microscopy (TEM) characterization was performed using a Talos™ F200X G2 TEM microscope (Thermo Scientific). Energy dispersive X-ray spectra (EDS) and elemental maps were collected along with HAADF-STEM (high angular annular dark field scanning transmission electron microscopy) micrographs using a four-detector Super-X Energy Dispersive system. Samples for analysis were ultrasonically dispersed in iso-propyl alcohol and a drop of the suspension was deposited on a holey carbon copper grid (300 mesh).

X-ray photoelectron spectroscopy (XPS) analyses were carried out in a UHV chamber ($10^{-9}/10^{-10}$ mbar) equipped with non-monochromatized Al radiation ($h\nu$ = 1486.6 eV, VSW-TA1) combined with a hemispherical electron/ion energy analyzer (VSW-HA100 with a 16-channel detector). The operating power of the X-ray source was 144 W (12 kV and 12 mA), and photoelectrons were collected normal to the sample surface, maintaining the angle between the analyzer axis and the X-ray source fixed at 54.5°. All samples were adsorbed on carbon tape, and the XPS spectra were acquired in a fixed analyzer transmission mode with a pass energy of 44.0 eV. CasaXPS software was used to analyze the spectra and a linear or Shirley function was used for background correction. The deconvolution of XPS spectra has been performed by applying a combination of Gaussian and Lorentzian functions (70/30 ratio) for N 1s and C 1s and Lorentzian asymmetric lineshapes for Al 2p and Pt 4f. All the binding energies (B.E.) were calibrated upon fixing C 1s of the carbon tape at 285.1 eV.[28]

Thermogravimetric analyses (TGA) were carried out using a SEIKO SII TG/DTA 7200 EXSTAR instrument (Chiba, Japan). Samples with masses between 3 and 5 mg were heated from 30 to 900 °C under a nitrogen flow of 200 mL $min^{-1}$, at a constant heating rate of 10 °C $min^{-1}$. The rate inflection temperatures corresponding to the different degradation steps were determined from the first-derivative thermogravimetric (DTG) curves. The final residue was evaluated at 900 °C.

High performance liquid chromatography (HPLC) analyses were carried out on an HPLC apparatus (Shimadzu), equipped with an Aminex HPX-87H chromatographic column (300 × 7.8 mm) (BIO-RAD) and an RID 10A detector. All analyses were carried out using sulfuric acid (0.005 M) as the eluent and applying a flow rate of 0.4 mL $min^{-1}$ and a column temperature of 35 °C. All organic compounds were quantified by means of calibration curves.

$^1$H NMR spectra were recorded with a Bruker AVANCE 400 spectrometer at room temperature using an Evans tube filled with $D_2O$.

Gas chromatography-mass spectrometry (GC-MS) was carried out with a GC-MS 2010SE apparatus (Shimadzu) equipped with a capillary column (VF WAXms, 30.0 m × 0.25 mm × 0.25 μm) and He as the carrier gas.

### 2.4 Catalysis

Catalytic hydrogenation reactions were conducted in a Teflon-lined stainless steel autoclave (70 mL) equipped with a magnetic stirrer, an electronic pressure controller and a thermocouple. The autoclave was heated by means of an external temperature-controlled oil bath. Typically, catalytic reactions were conducted as follows: the autoclave was charged with the catalyst (20 mg) and then sealed and evacuated. Afterwards, a deaerated water solution of the substrate (20 mL, 57.5 mM) was introduced into the autoclave by suction, followed by heating it to the desired temperature. Once the reaction temperature was reached, the autoclave was pressurized with hydrogen (25 bar) and magnetically stirred for the desired reaction time. The autoclave was then cooled to 10 °C by means of a water–ice bath, excess gas was vented off and the solid catalyst was separated from water solution by centrifugation. The clear water solution was analysed by HPLC, $^1$H NMR spectroscopy, GC-MS spectrometry and ICP-OES. Recycling experiments were carried out upon washing the separated catalyst with water, followed by centrifugation. The wet catalyst was then redispersed in water (20 mL), which contained the substrate (1.15 mmol). The obtained suspension was transferred to the evacuated autoclave by suction. The autoclave was then successively sealed, slowly flushed with hydrogen for 2 minutes, heated to the desired temperature and then pressurized with hydrogen (25 bar) followed by magnetic stirring of the reaction suspension. Catalysts **1** and **2**, recovered and subjected to TEM, XPS and PXRD analyses were extensively rinsed with water and then vacuum-dried at 50 °C.

## 3. Results and discussion

### 3.1 Synthesis and characterization of the materials

The synthesis approach of $SiO_2$ spheres and CTF@$SiO_2$ spheres is presented in Fig. 1. Following a previously reported

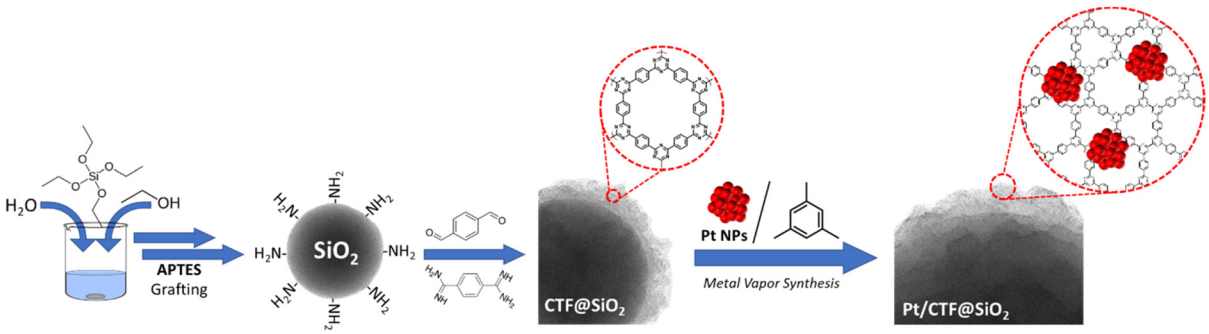


**Fig. 1** Synthesis method for **1**.

procedure,[27] uniform $SiO_2$ spheres with diameters in the range of 240–260 nm were prepared. The $SiO_2$ spheres were treated with (3-aminopropyl)triethoxysilane (APTES) and the amino groups present at their surface were further used to anchor terephthalaldehyde by a Schiff base reaction (see FT-IR spectra reported in Fig. S1). The aldehyde monomers were then reacted with 1,4-terephthalamidine dihydrochloride at the surface of the material and finally, both precursors were added simultaneously to obtain the final CTF@$SiO_2$.

Ultrafine Pt NPs were synthesized as ligand-free particles in their reduced form by the MVS approach[19,29] and supported on either CTF@$SiO_2$ or $SiO_2$ to obtain composites **1** and **2**, respectively, that were then stored at room temperature, under a dry air atmosphere. The quantitative deposition of Pt NPs on the supports was verified by ICP-OES analysis, which gave a final Pt content of 2.0 wt% for both **1** and **2**.

Transmission electron microscopy analysis was performed to investigate the structural and morphological features of both the pristine supports CTF@$SiO_2$ and $SiO_2$ (Fig. 2(a)–(c), and Fig. S2, respectively) and of the corresponding derived catalysts **1** and **2** (Fig. 3 and S3, and Fig. S4, respectively). TEM analysis of the CTF@$SiO_2$ and $SiO_2$ support showed in both samples the presence of $SiO_2$ spheres with a very homogeneous size distribution, ranging from 240 to 260 nm in diameter. In addition, CTF@$SiO_2$ exhibited the additional presence of a rough organic shell (CTF) 25 to 30 nm thick covering the entire surface of the $SiO_2$ spheres. HAADF-STEM/EDS element map analysis confirmed the presence of both carbon

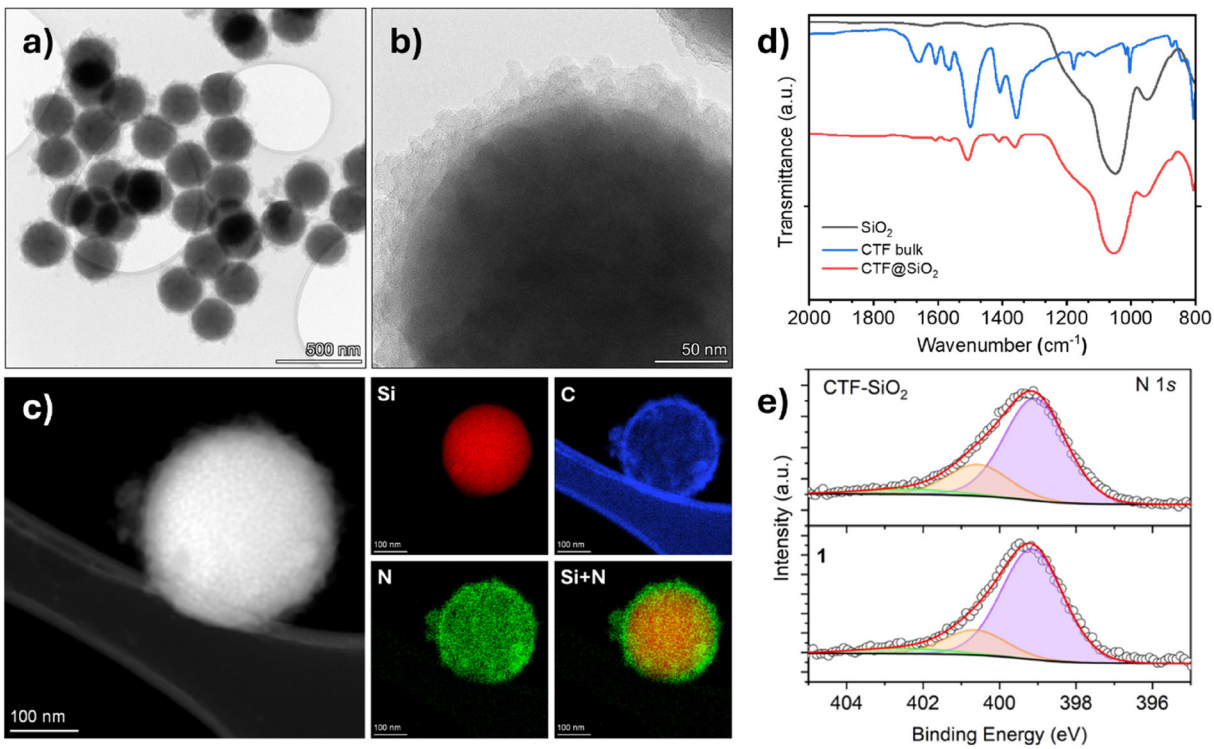


**Fig. 2** Representative TEM micrographs of CTF@$SiO_2$ acquired at low and high magnification, (a) and (b), respectively; HAADF-STEM/EDS elemental map, (c); FT-IR spectra of $SiO_2$, CTF and CTF@$SiO_2$, (d); and high resolution N 1s XPS spectra for CTF@$SiO_2$, (upper part) and **1** (lower part), (e).

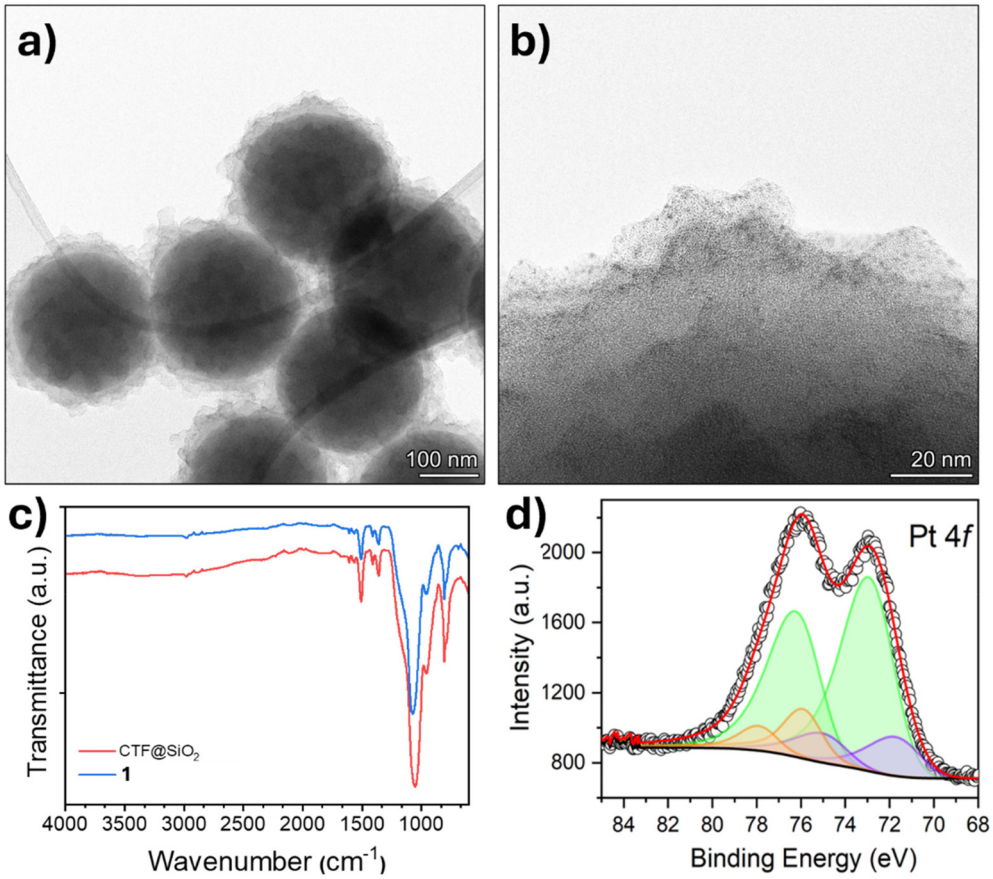


**Fig. 3** Structural characterization of **1**: representative TEM micrographs acquired at low (a) and high magnification (b), respectively; FT-IR spectra (c); and high resolution XPS spectra in the Pt 4f core region showing also the Al 2p photoelectron peaks (orange peaks) originating from a perforated aluminium foil that covered **1** during drying under reduced pressure (d).

and nitrogen atoms at the outer shell of the CTF-$SiO_2$ spheres. Interestingly, no formation of segregated organic aggregates outside of the $SiO_2$ surface was observed. Moreover, FT-IR spectra of the CTF@$SiO_2$ support (Fig. 2(d)), as well as of the $SiO_2$ functionalization intermediates (*i.e.* $SiO_2$ surface reaction with APTES and the further modification with TPA, Fig S4), confirmed that the growth of the organic framework successfully occurred at the surface of the silica spheres. The obtained CTF@$SiO_2$ exhibited characteristic vibrations of the triazine units at 1523 and 1367 $cm^{-1}$, ascribed to C═N stretching vibrations that are identical to those observed for the bare CTF bulk material. Moreover, as expected, the Si–O stretching frequency at 1078 $cm^{-1}$ was observed in the examined samples (Fig. 2(d) and S1).

To get further insight into the structural features of CTF@$SiO_2$, X-ray Photoelectron Spectroscopy (XPS) analyses were carried out (Fig. 2e and S5). Survey spectra of the support showed the presence of the expected elemental composition (*i.e.* Si, C, N and O). High-resolution N 1s XPS spectra reported in Fig. 2(e) revealed the main component centred at a binding energy (B.E.) of 399.0 eV, which proves the presence of pyridinic nitrogen (C═N–C) stemming from CTF triazine moieties. In addition, a second N 1s photoelectron contribution at B.E. of 400.7 eV and a shakeup component B.E. of 402.5 eV also confirmed the presence of oxidized nitrogen atoms in the CTF framework.[30–32] The Si 2p photoelectron spectrum of both supports was characterized by a single contribution at a B.E. of *ca.* 103.7 eV, which corroborated the presence of $SiO_2$.[33] While bare $SiO_2$ microspheres exhibited a specific surface area (SSA) of 16 $m^2$ $g^{-1}$, the presence of CTF on the surface of the $SiO_2$ spheres (CTF@$SiO_2$) significantly increased the SSA to 33 $m^2$ $g^{-1}$ (Table S2). Very low porosity was observed for both materials (Fig. S6) and the H3 type hysteresis loop indicates slit-shaped pores, which are typical of aggregates of plate-like particles.

TEM analysis of both MVS-derived **1** (Fig. 3a and b, and Fig. S3) and **2** (Fig. S4) showed no appreciable alterations in the structural and morphological properties of the corresponding pristine supports. TEM analysis at high magnifications along with HAADF-STEM/EDS platinum maps showed the presence of highly dispersed Pt-NPs along the support surface, falling in the sub-nanometer range (<1.3 nm) for both 1 and 2 (Fig. 3(b), S3, and S4, respectively). Similar results were previously reported by depositing pre-formed MVS-derived Pt/mesitylene NPs on different carbon-based supports.[19,29]

The FT-IR spectrum of **1** (Fig. 3(c)) was very similar to that recorded for pristine CTF@$SiO_2$, indicating the absence of any

significant support modification during the immobilization of Pt NPs onto CTF-$SiO_2$.

XPS analysis of **1** showed the presence of the expected elemental composition (*i.e.* Si, C, N, O and Pt) (Fig. S7) and the corresponding N 1s photoelectron spectrum (Fig. 2(e)) showed the same feature as that found for CFT@$SiO_2$. In addition, the B.E. for the pyridinic nitrogen atom at a B.E. of 399.1 eV is almost identical to that found for CTF@$SiO_2$ (399.0 eV), indicating that no Pt–N interaction was detected between the surface Pt and nitrogen atoms of CTF, likely due to the low Pt loading (2 wt% Pt, see section 2.2). Interestingly, the Si 2p photoelectron peak of **1** and **2** exhibited the same characteristic B.E. of 103.7 eV, but differed notably in intensity, which clearly suggests the presence of a CTF layer entirely covering the $SiO_2$ nanospheres (Fig. S5). Pt 4f XPS spectrum shown for **1** in Fig. 3(d) contains two contributions that correspond to Pt (II), which is the major fraction (83.3 at%), at a B.E. of 72.3 eV (Pt $4f_{7/2}$) and Pt(0) at a B.E. of 71.1 eV (Pt $4f_{7/2}$).[34,35] Interestingly, the Pt 4f photoelectron spectrum of **2** is characterized by the presence of a lower percentage of surface Pt(II) atoms (*i.e.* 68.5 at%, Table S1), which might indicate easier oxidation of surface Pt atoms in **1** due to electron donation originating from CTF nitrogen atoms, compared to **2** (*i.e.* Pt(II) 68.5 at%, Table S1, Fig. S9).

The thermal behaviour of **1** and of the corresponding support was investigated by TGA under a nitrogen atmosphere (Fig. 4).

The TGA curve of pristine silica ($SiO_2$) showed a minor weight loss of about 6 wt% up to 900 °C mainly due to the desorption of physically adsorbed water below 150 °C (about 2%) and the condensation of surface hydroxyl groups above 200 °C.[36] In contrast, silica coated with the covalent triazine-based framework (CTF@$SiO_2$) showed an initial weight loss starting at around 200 °C and continuing up to 600 °C, followed by a second step between 600 and 900 °C, consistent with the decomposition of the organic framework as observed for the bulk CTF reference. The overall mass loss of this sample (≈18% at 900 °C) corresponds to a CTF content of about 20–25 wt%. **1** showed a similar decomposition profile to that of CTF@$SiO_2$, with a slightly higher total weight loss (≈19% at 900 °C), confirming a comparable amount of CTF.

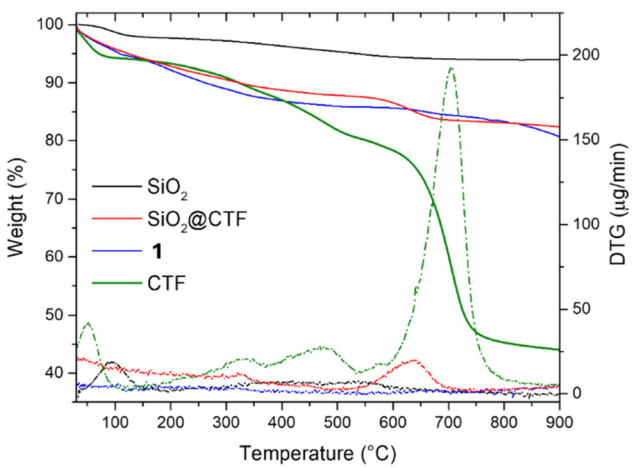


**Fig. 4** Thermogravimetric analysis of $SiO_2$, CTF@$SiO_2$, **1**, and bulk CTF material.

### 3.2 Catalysis in water

Catalysts **1** and **2** have been screened in water for the hydrogenation of **2,3-BDO** and **PyA** by applying a substrate to a Pt molar ratio of 561. The reaction products were analyzed by means of HPLC, $^1$H NMR spectroscopy and GC-MS spectrometry. All obtained products were quantified by HPLC using calibration curves for each compound. All catalytic reactions were carried out twice and the reported results, compiled in Table 1, are average values. To avoid diffusion-controlled reactions, the stirring speed of the autoclave (*i.e.* magnetic stirring) was optimized to 1000 rpm. Also, the hydrogen pressure used in catalyst screening (*i.e.* from 5 to 30 bar) was optimized to 25 bar (Table 1). The relatively high hydrogen pressure needed to obtain a rational conversion of intermediate A into B and C is due to the low solubility of hydrogen in water.[37] In contrast, the conversion of **2,3-BDO** in intermediate A occurs at high conversion even at low hydrogen pressure (5 bar) (Table 1).

Irrespective of the catalyst used, the hydrogenation of **2,3-BDO** was found to give three reaction products, namely 3,4-dihydroxy-3,4-dimethylhexa-2,5-dione (**A**), 3-hydroxy-butan-2-one (**B**) and butane-2,3-diol (**C**), whereas in the absence of the Pt-based catalyst, no substrate conversion occurred (Table 1, entry 1). Upon carrying out catalytic reactions with either catalyst at two different reaction temperatures (*i.e.* 85 and 105 °C) the stepwise hydrogenation reaction from **2,3-BDO** to butane-2,3-diol was obvious.[38–42] At 85 °C **2,3-BDO** was converted first into dimer **A**, which was successively converted into **B**, as confirmed by catalytic reactions conducted at the latter temperature at different reaction times (Table 1, entries 2, 3 and 9). The chemical nature of dimer **A** has been proved by $^1$H and $^{13}$C{$^1$H} NMR spectroscopy (Fig. S10 and S11) as well as by MS analysis (Fig. S12). This dimer formation contrasts with that reported for **2,3-BDO** occurring in dichloromethane in the presence of Pt NPs decorated with the nitrogen atom containing ligands.[12] The formation of compound **A** occurred by reductive coupling of two molecules of **2,3-BDO** in the presence of NPs' surface Pt(0) atoms, which act as a reducing agent, while water is needed to protonate the deprotonated diol intermediate, yielding **A** (Scheme S1).[43,44] The experimental fact that in the absence of hydrogen, **2,3-BDO** was not converted into A, whereas in the presence of a relatively low hydrogen pressure (5 bar) a high **2,3-BDO** conversion into A (95%, Table 1, entry 5) was observed, indicates that hydrogen is needed to regenerate Pt(0) NPs' surface atoms.

At 85 °C, only small amounts of C (2.2%) were obtained with the most active catalyst **1** after a reaction time of 3 h (Table 1, entry 9) (Fig. S13). Upon increasing the reaction temperature to 105 °C, a notable conversion of **2,3-BDO** into C (23.2%) was achieved for **1** (Table 1, entry 12), while an almost quantitative formation of C (99.1%) was achieved after a reac-

 

**Table 1** **1** and **2**-catalyzed hydrogenation of **2,3-BDO** and **PyA** in water

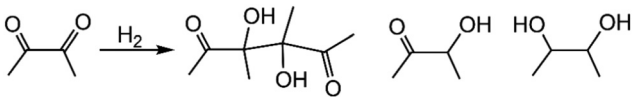


**2,3-BDO** **A** **B** **C**

| Entry[a] | Catalyst | *t* (h) | *T* (°C) | Conv. substrate (%) | A[b] (%) | B (%) | C (%) [*meso*/*rac*] | D (%) | E (%) | F (%) | G (%) |
|---|---|---|---|---|---|---|---|---|---|---|---|
| 1 | — | 1 | 85 | — | — | — | — | | | | |
| 2 | **1** | 0.5 | 85 | 93.1 | 65.9 | 33.6 | 0.5 | | | | |
| 3 | **1** | 1 | 85 | 96.5 | 52.2 | 45.9 | 1.9 | | | | |
| 4[c] | **1** | 1 | 85 | — | — | — | — | | | | |
| 5[d] | **1** | 1 | 85 | 95.0 | 75.2 | 24.8 | — | | | | |
| 6[e] | **1** | 1 | 85 | 97.0 | 68.2 | 31.8 | — | | | | |
| 7[f] | **1** | 1 | 85 | 98.0 | 60.0 | 39.0 | 1.0 | | | | |
| 8[g] | **1** | 1 | 85 | 97.5 | 51.0 | 47.9 | 1.1 | | | | |
| 9 | **1** | 3 | 85 | 100.0 | 35.2 | 62.6 | 2.2 | | | | |
| 10 | **2** | 1 | 85 | 96.5 | 76.8 | 23.2 | - | | | | |
| 11 | **2** | 3 | 85 | 99.5 | 44.5 | 55.5 | - | | | | |
| 12 | **1** | 3 | 105 | 100.0 | — | 76.8 | 23.2 | | | | |
| 13 | **1** | 15 | 105 | 100.0 | — | 0.9 | 99.1/[3/4] | | | | |
| 14 | **2** | 3 | 105 | 100.0 | 2.1 | 95.5 | 2.4 | | | | |
| 15 | **2** | 15 | 105 | 100.0 | — | 80.9 | 19.1/[3/4] | | | | |
| 16[h] | **2** | 3 | 105 | 89.0 | 20.0 | 79.0 | 1.0 | | | | |
| 17[h] | **1** | 3 | 105 | 100.0 | | 77.0 | 23.0 | | | | |
| 18[i] | **1** | 3 | 105 | 100.0 | | 77.3 | 22.7 | | | | |
| 19[j] | **1** | 3 | 105 | 100.0 | | 77.8 | 22.2 | | | | |

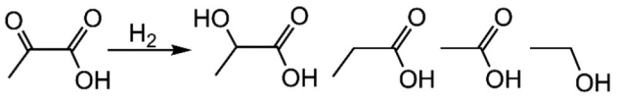


**PyA** **D** **E** **F** **G**

| | | | | | | | | | | | |
|---|---|---|---|---|---|---|---|---|---|---|---|
| 20 | — | 1 | 105 | — | — | — | — | — | — | — | — |
| 21[c] | **1** | 1 | 105 | — | | | | — | — | — | — |
| 22[f] | **1** | 1 | 105 | 77.2 | | | | 92.9 | 2.2 | 1.9 | 3.0 |
| 23 | **1** | 1 | 105 | 85.6 | — | — | — | 90.9 | 2.9 | 2.2 | 4.0 |
| 24[g] | **1** | 1 | 105 | 86.5 | | | | 89.2 | 2.9 | 3.9 | 4.0 |
| 25 | **2** | 1 | 105 | 32.4 | — | — | — | 83.7 | 5.5 | 6.9 | 3.9 |
| 26 | **2** | 2 | 105 | 52.8 | | | | 91.6 | 2.9 | 2.1 | 3.4 |
| 27[h] | **1** | 1 | 105 | 86.7 | | | | 90.9 | 5.9 | 2.7 | 0.5 |
| 28[i] | **1** | 1 | 105 | 85.6 | | | | 90.7 | 5.5 | 3.8 | — |
| 29[j] | **1** | 1 | 105 | 85.1 | | | | 89.9 | 5.0 | 5.1 | — |

[a] Catalytic conditions: catalyst (20.0 mg, 2.05 μmol of Pt), substrate (1.15 mmol), water (20.0 mL), p($H_2$) (25 bar). [b] (*rac*/*meso* ratio close to 1). [c] Without $H_2$. [d] *p*($H_2$) (5 bar). [e] *p*($H_2$) (10 bar). [f] *p*($H_2$) (20 bar). [g] *p*($H_2$) (30 bar). [h] 1st recycling. [i] 2nd recycling. [j] 3rd recycling.

tion lasting 15 h (Table 1, entry 13) (Fig. S14 and S15). In contrast, **2** led to only 19.1% of C under these conditions (Table 1, entry 15 *vs.* 13). Irrespective of the catalyst, both stereoisomers of C (*meso*/*rac*) were obtained in a 3 : 4 molar ratio (Table 1).

The hydrogenation reactions of **PyA**[45,46] conducted in water at 105 °C and with a hydrogen pressure of 25 bar gave lactic acid (**D**) as the major compound, irrespective of the catalyst used (Fig. S16 and S17) (Table 1, entries 20–29). Along with lactic acid, propionic (**E**) and acetic acid (**F**), as well as trace amounts of ethanol (**G**) were formed when fresh catalysts were used. Propionic acid was obtained from lactic acid by a dehydration/hydrogenation step.[47–51] Acetic acid and ethanol are mainly obtained upon decarboxylation of **PyA**.[52,53] Analogously to the results obtained in the hydrogenation of **2,3-BDO**, **1** showed significantly higher catalytic activity compared to **2** (Table 1, entry 23 *vs.* 25) along with a higher lactic acid selectivity (90.9 (**1**) *vs.* 83.7 (**2**)), due to the formation of lower amounts of propionic and acetic acid.

The significantly higher catalytic hydrogenation activity of **1** compared to **2** is the consequence of efficient surface Pt–N interactions between NPs' surface Pt(0) atoms (Lewis acid sites) and support-nitrogen atoms (Lewis base sites). These Lewis acid–base couples foster the heterolytic hydrogen splitting, which leads to the formation of surface Pt-hydride species, which are the real catalytic species, operative in hydrogenation reactions when polar functional groups, such as C=O bonds, are converted to the corresponding alcohol functionality.[54]

The stability of both catalysts during hydrogenation reactions in water was verified by carrying out recycling experi-

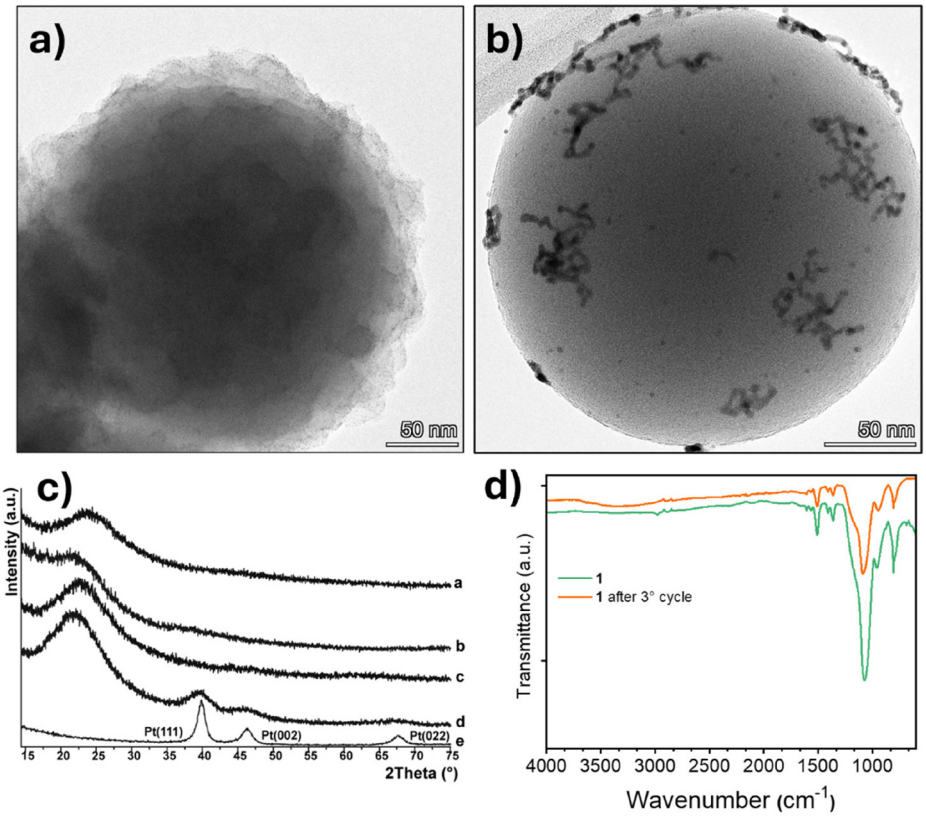


**Fig. 5** Representative TEM micrograph of recovered **1** (after 15 h reaction time at 105 °C (a) and recovered **2** (after 3 h reaction time at 105 °C (b)); PXRD spectra acquired at room temperature for **1** and **2** (c)): as-synthesized **1** (a); recovered **1** (b); as-synthesized **2** (c), recovered **2** (d) and pristine Pt-NPs (e); and FT-IR analysis of as-synthesized **1** (green) and recovered **1** after three catalytic cycles (orange) (Table 1 entry 19).

ments, ICP-OES analyses of the reaction solution after hot filtration, and the structural characterization of the recovered catalysts. As a result, recycling experiments conducted with **1** and **2** under identical catalytic conditions proved that **1** gave almost identical substrate conversion for three consecutive catalytic reactions, using **2,3-BDO** as the substrate (Table 1, entries 17–19), which is in stark contrast to the drop in catalytic activity found for **2**, already after the first recycling experiment (Table 1, entry 16 *vs.* 14). In addition, in consecutive catalytic reactions using **PyA** as the substrate, **1** also showed an almost identical conversion with high lactic acid selectivity of roughly 90% maintained throughout four consecutive catalytic runs (Table 1, entries 23 *vs.* 27–29). ICP-OES analyses of the hot filtered solutions resulted in low leaching for both catalysts, which was close to the detection limit of the instrument (<2 ppb). TEM analyses of recovered **1** and **2** (*i.e.* after 15 h reaction time at 105 °C (**1**) and after 3 h reaction time at 105 °C (**2**)) are shown in Fig. 5a and b, respectively, and confirm the high stability of **1** against sintering (Pt NPs of the recovered catalyst showed a comparable size to the as-synthesized one). On the other hand, strong sintering of the Pt NPs was observed in the case of **2** (Fig. 5(b)). In agreement with the TEM results, PXRD spectra acquired for recovered **1** and **2** showed the presence of the characteristic diffraction peaks only in the case of **2** assigned to *fcc* Pt (*i.e.* Pt (111) at 39.6 ($2\Theta$) and Pt (200) at 46.4 ($2\Theta$)) (Fig. 5(c)), (Fig. 5c), trace d; the PXRD pattern of pristine Pt-NPs is shown in Fig. 5c, trace (e). This experimental result confirms strong sintering of Pt NPs in **2** (*i.e.* average NPs' size of 2.8 nm has been determined by the Debye–Scherrer method[46] based on the Pt(111) Bragg reflex). The TGA curve of recovered **1** (*i.e.* after four catalytic cycles) (Fig. S18) is almost identical to that of as-synthesized **1**, confirming the high stability of the organic CTF phase under real catalytic conditions. The temperature corresponding to the maximum degradation rate (DTG peak) was observed at approximately 700 °C, which is comparable to that of pristine CTF, but shifted relative to CTF@$SiO_2$, where the peak appeared at around 640 °C. The high stability of $SiO_2$-supported CTF under the chosen catalytic conditions is further confirmed by the identity of the FT-IR spectra of recovered **1** (after 3 catalytic cycles) and as-synthesized **1** (Fig. 5(d)).

## 4. Conclusion

We showed that sub-nanometric-sized Pt NPs (<1.3 nm), synthesized by the MVS technique and supported onto a covalent triazine (CTF) framework, which entirely covers $SiO_2$ nanospheres (**1**), were highly active in the hydrogenation of **2,3-BDO** and **PyA** in water. Butane-2,3-diol and lactic acid were

 

selectively obtained under relatively mild reaction conditions (*i.e.* *T*, 105 °C and $p(H_2)$, 25 bar). Related catalytic systems hydrogenate **2,3-BDO** mainly to 3-hydroxy-2-butanone using ethanol, toluene, iso-propanol or dichloromethane as the reaction medium[40–42] and **PyA** is hydrogenated in water to lactic acid using Ru-based catalysts.[45,54] The crucial role of CTF in electron donation to surface Pt(0) centers, favouring the formation of Pt–H species, which are the dominant catalytic species for C=O bond hydrogenation and in stabilizing the Pt-NPs under real catalytic reaction conditions, has been proved by: (i) comparison of the catalytic activity of Pt NPs on $SiO_2$ (**2**) (*i.e.* Pt NPs synthesized by the same method as **1**, thus showing the same Pt dispersion on the support surface): catalyst **1** exhibited higher catalytic activity than **2**, irrespective of the substrate, but also higher chemoselectivity mainly in the hydrogenation of **PyA** to lactic acid (Table 1, <90%); (ii) TEM and PXRD analyses conducted on recovered **1** and **2**, which confirmed that in contrast to **1**, **2** experienced a notable NP sintering even after relatively short reaction times (3 h); and (iii) recycling experiments conducted with **1**, which exhibited almost identical catalytic performance in four successive catalytic reactions, regardless of the substrate used.

## Conflicts of interest

There are no conflicts to declare.

## Data availability

The data supporting this article have been included as part of the supplementary information (SI). Supplementary information is available. See DOI: https://doi.org/10.1039/d5dt02604k.

## Acknowledgements

The authors thank the Italian MUR through the PRIN2022 project "HYPOCOF: Hybrid Porous Materials for Eco-sustainable Catalytic Organic Processes" (20222H43S2; CUP B53C24005950006).

## References

1 Y. Yusran, H. Li, X. Guan, Q. Fang and S. Qiu, *EnergyChem*, 2020, **2**, 100035.
2 H. El-Kaderi, J. R. Hunt, J. L. Mendoza-Cortez, A. P. Cote, R. E. Taylor, M. O'Keeffe and O. M. Yaghi, *Science*, 2007, **316**, 268–272.
3 S. S. A. Shah, M. S. Javed, T. Najam, M. A. Nazir, A. ur Rehman, A. Rauf, M. Sohail, F. Verpoort and S. J. Bao, *Mater. Today*, 2023, **67**, 229–255.
4 V. Sharma, M. Nemiwal and D. Kumar, *Mini-Rev. Org. Chem.*, 2022, **19**, 815–825.
5 N. Tahir, C. Krishnaraj, K. Leus and P. Van Der Voort, *Polymers*, 2019, **11**, 1326.
6 M. Liu, L. Guo, S. Jin and B. Tan, *J. Mater. Chem. A*, 2019, **7**, 5153–5172.
7 P. Puthiaraj, Y. R. Lee, S. Zhang and W. S. Ahn, *J. Mater. Chem. A*, 2016, **4**, 16288–16311.
8 A. Imehoff, M. Vennewald and R. Palkovits, *Angew. Chem., Int. Ed.*, 2023, **62**, e202212015.
9 Y. Li, C. Lai, S. Liu, Y. Fu, L. Qin, M. Xu, D. Ma, X. Zhou, F. Xu, H. Liu, L. Li, Q. Sun and N. Wang, *J. Mater. Chem. A*, 2023, **11**, 2070–2091.
10 D. Ma, X. Huo, C. Lai, H. Yi, L. Zeng, F. Xu, H. Yan, X. Zhou, X. Fan, L. Tang and M. Yan, *Appl. Catal., B*, 2026, **381**, 125894.
11 D. Ma, C. Lai, H. Yi, X. Huo, L. Li, M. Zhang, F. Xu, H. Yan, S. Hu and Y. Luo, *Coord. Chem. Rev.*, 2025, **522**, 216241.
12 X. Zhu, F. Guo, Q. Yang, H. Mi, C. Yang and J. Qui, *J. Power Sources*, 2021, **506**, 230224.
13 M. Gao, G. He, X. Long, S. Wang, Z. Guo, Z. Dong and K. Yuan, *ACS Sustainable Chem. Eng.*, 2024, **12**, 14732–14746.
14 T. He, L. Liu, G. Wu and P. Chen, *J. Mater. Chem. A*, 2015, **3**, 16235–16241.
15 J. Zhang, G. Zhang, L. He, Y. Shi, R. Miao, Y. Zhu and Q. Guan, *Appl. Surf. Sci.*, 2021, **570**, 150881.
16 L. Liao, M. Li, Y. Yin, J. Chen, Q. Zhong, R. Du, S. Liu, Y. He, W. Fu and F. Zheng, *ACS Omega*, 2023, **8**, 4527–4542.
17 H. Vardhan, G. Rummer, A. Deng and S. Ma, *Membranes*, 2023, **13**, 696.
18 E. Pitzalis, R. Psaro and C. Evangelisti, *Inorg. Chim. Acta*, 2022, **533**, 120782.
19 X. T. Nguyen, E. Kitching, T. Slater, E. Pitzalis, J. Filippi, W. Oberhauser and C. Evangelisti, *Catalysts*, 2024, **14**, 798.
20 Y. Bai, H. Feng, N. Liu and X. Zhao, *Energies*, 2023, **16**, 5802.
21 M. Dusselier, P. Van Wouwe, A. Dewaele, E. Makshina and B. F. Sels, *Energy Environ. Sci.*, 2013, **6**, 1415–1442.
22 J. A. Slipszenko, S. P. Griffiths, P. Johnston, K. E. Simons, W. A. H. Vermeer and P. B. Wells, *J. Catal.*, 1998, **179**, 267–276.
23 Y. Nagai, S. Morooka, N. Matsubayasi and M. Nakahara, *J. Phys. Chem. A*, 2004, **108**, 11635–11643.
24 D. R. Aireddy and K. Ding, *ACS Catal.*, 2022, **12**, 4707–4723.
25 E. A. Redina, K. V. Vikanova, G. I. Kapustin, I. V. Mishin, O. P. Tkachenko and L. M. Kustov, *Eur. J. Org. Chem.*, 2019, 4159–4170.
26 N. Wang, G. Cheng, L. Guo, B. Tan and S. Jin, *Adv. Funct. Mater.*, 2019, **29**, 1904781.
27 K. Wang, L.-M. Yang, X. Wang, L. Guo, G. Cheng, C. Zhang, S. Jin, B. Tan and A. Cooper, *Angew. Chem., Int. Ed.*, 2017, **56**, 14149.
28 A. J. Barlow, S. Popescu, K. Artyushkova, O. Scott, N. Sano, J. Hedley and P. J. Cumpson, *Carbon*, 2016, **107**, 190–197.
29 W. Oberhauser, C. Evangelisti, R. P. Jumde, R. Psaro, F. Vizza, M. Bevilacqua, J. Filippi, B. F. Machado and P. Serp, *J. Catal.*, 2015, **325**, 111–117.

30 X. Zhu, C. Tian, S. M. Mahurin, S. Chai, C. Wang, S. Brown, G. M. Veith, H. Luo, H. Liu and S. Dai, *J. Am. Chem. Soc.*, 2012, **134**, 10478–10484.
31 Z. Luo, S. Lim, Z. Tian, J. Shang, L. Lai, B. MacDonald, C. Fu, Z. Shen, T. Yu and J. Lin, *J. Mater. Chem.*, 2011, **21**, 8038–8044.
32 A. Mohtasebi, T. Chowdhury, L. H. Hsu, M. C. Biesinger and P. Kruse, *J. Phys. Chem. C*, 2016, **120**, 29248–29263.
33 A. Y. Lee, C. J. Powell, J. M. Gorham, A. Morey, J. H. J. Scott and R. J. Hanisch, *Data Sci. J.*, 2024, **23**, 45.
34 M. G. Bancroft, I. Adams, L. L. Coatswirth, D. C. Bennewitz, J. D. Brown and W. D. Westwood, *Anal. Chem.*, 1975, **47**, 586–588.
35 W. Oberhauser, C. Evangelisti, X. T. Nguyen, J. Filippi, L. Poggini, L. Capozzoli, G. Manca, E. A. Kitching, T. J. A. Slater and M. Danale, *Inorg. Chem.*, 2024, **63**, 22912–22922.
36 F. Kunc, V. Balhara, Y. Sun, M. Daroszewska, Z. J. Jakubek, M. Hill, A. Brinkmann and L. J. Johnston, *Analyst*, 2019, **144**, 5589–5599.
37 Z. Zhu, Y. Cao, Z. Zheng and D. Chen, *Energies*, 2022, **15**, 5021.
38 H. Duan, Y. Yamada and S. Sato, *Catal. Commun.*, 2017, **99**, 53–56.
39 N. Carrara, J. Badano, N. Bertero, G. Torres, C. Betti, L. Martinez-Bovier, M. Quiroga and C. Vera, *J. Chem. Technol. Biotechnol.*, 2014, **89**, 265–275.
40 N. Carrara, J. M. Badano, F. Coloma-Pascual, C. Vera and M. Quiroga, *Chem. Pap.*, 2017, **71**, 1669–1683.
41 R. P. K. Wells, N. R. McGuire, X. Li, R. L. Jenkins, P. J. Collier, R. Whyman and G. J. Hutchings, *Phys. Chem. Chem. Phys.*, 2002, **4**, 2839–2845.
42 M. Studer, V. Okafor and H.-U. Blaser, *Chem. Commun.*, 1998, 1053–1054.
43 Y.-S. Yang, Z.-L. Shen and T.-P. Loh, *Org. Lett.*, 2009, **11**, 2213–2215.
44 B. Cao, S. Li, W. Kong, J. Guo, Z. Tian and G. Zhang, *Inorg. Chem. Commun.*, 2020, **121**, 108227.
45 R. Luque and J. H. Clark, *Catal. Commun.*, 2010, **11**, 928–931.
46 G. Jones and S. J. Jenkins, *J. Am. Chem. Soc.*, 2008, **130**, 14483–14492.
47 X. Li, J. Pang, J. Zhang, C. Yin, W. Zou, C. Tang and L. Dong, *Ind. Eng. Chem. Res.*, 2019, **58**, 101–109.
48 X. Li, Z. Zhai, C. Tang, L. Sun, Y. Zhang and W. Bai, *RSC Adv.*, 2016, **6**, 62252–62262.
49 Z. Huo, J. Xiao, D. Ren, F. Jin, T. Wang and G. Yao, *Green Chem.*, 2017, **19**, 1308–1314.
50 S. Liu, H. Feng, T. Li, Y. Wang, N. Rong and W. Yang, *Green Chem.*, 2020, **22**, 7468–7475.
51 Y. Nagai, C. Wakai, N. Matubayasi and M. Nakahara, *Chem. Lett.*, 2003, **32**, 310–311.
52 D. R. Aireddy and K. Ding, *ACS Catal.*, 2022, **12**, 4707–4723.
53 U. Holzwarth and N. Gibson, *Nat. Nanotechnol.*, 2011, **6**, 534.
54 W. Oberhauser, L. Poggini, L. Capozzoli, M. V. Pagliaro, S. Coiai and C. Evangelisti, *Inorg. Chem.*, 2025, **64**, 14382–14394.